International Journal of Mass Spectrometry 302 (2011) 85–92

Contents lists available at ScienceDirect

International Journal of Mass Spectrometry

journal homepage: www.elsevier.com/locate/ijms

Hydrophobic peptides affect binding of calmodulin and Ca^{2+} as explored by H/D amide exchange and mass spectrometry

Justin B. Sperry[b,1], Richard Y-C. Huang[a], Mei M. Zhu[c,1], Don L. Rempel[a], Michael L. Gross[a,*]

[a] Department of Chemistry, Washington University in St. Louis, One Brookings Drive, POBox 1134, St. Louis, MO 63130, United States
[b] BioTherapeutics Research and Development, Pfizer Inc., Chesterfield, MO 63017, United States
[c] Millennium Pharmaceuticals, Inc., Cambridge, MA, United States

ARTICLE INFO

Article history:
Received 23 May 2010
Received in revised form 5 August 2010
Accepted 16 August 2010
Available online 24 August 2010

Keywords:
Hydrogen/deuterium exchange
PLIMSTEX
Calmodulin
Myosin light-chain kinase (MLCK)
Melittin
Mastoparan
LC–MS

ABSTRACT

Calmodulin (CaM), a ubiquitous intracellular sensor protein, binds Ca^{2+} and interacts with various targets as part of signal transduction. Using hydrogen/deuterium exchange (H/DX) and a high-resolution PLIMSTEX (protein–ligand interactions by mass spectrometry, titration, and H/D exchange) protocol, we examined five different states of calmodulin: calcium-free, calcium-loaded, and three states of calcium-loaded in the presence of either melittin, mastoparan, or skeletal myosin light-chain kinase (MLCK). When CaM binds Ca^{2+}, the extent of H/DX decreased, consistent with the protein becoming stabilized upon binding. Furthermore, Ca^{2+}-saturated calmodulin exhibits increased protection when bound to the peptides, forming high-affinity complexes. The protocol reveals significant changes in EF hands 1, 3, and 4 with saturating levels of Ca^{2+}. Titration of the protein using PLIMSTEX provides the Ca^{2+}-to-calmodulin binding affinity, which agrees well with previously reported values. The affinities of calmodulin to Ca^{2+} increase by factors of 300 and 1000 in the presence of melittin and mastoparan, respectively. A modified PLIMSTEX protocol whereby the protein is digested to component peptides gives a region-specific titration. The resulting titration data show a decrease in the root mean square fit of the residuals, indicating a better fit of the data. The global H/D exchange results and those obtained in a region-specific way provide new insight into the Ca^{2+}-binding properties of this well-studied protein.

1. Introduction

Calcium ions (Ca^{2+}) play a vital role in biological functions of higher organisms, particularly in signal transduction [1–3]. Calcium channels regulate the [Ca^{2+}] inside the cell to 0.1–1.0 μM, from an extracellular concentration of 1.0 mM [4]. Of the over 500 Ca^{2+}-binding proteins identified, many are responsible for monitoring the intracellular Ca^{2+} concentration and communicating this signal to a binding partner [5]. Calmodulin (CaM) is a highly conserved, small (148 amino acids in eukaryotes), acidic (pI 3.9–4.3), ubiquitous protein that functions as an intracellular sensor protein using Ca^{2+} [6–9]. CaM when it is calcium-bound can bind up to 300 target proteins and/or peptides in signal transduction pathways [4].

Calcium-binding proteins contain a helix-loop-helix motif [10] called an EF hand that consists of a nine-amino acid residue helix, a 12-residue loop, and then another eight-residue helix. The loop contains highly conserved Asp, Gly, and Glu in position 1, 6, and 12 [5]. CaM consists of two globular domains at the N- and C-termini, each containing two EF hands; the globular domains are connected by a central α-helix. The Ca^{2+}-bound form of CaM is dumbbell-shaped with two Ca^{2+} ions bound in each domain. The structure of Ca^{2+}-loaded CaM determined by X-ray crystallography reveals the overall dumbbell shape of the protein and an α-helix connecting both domains [11,12]. A more recent NMR structure reveals that the central linker is highly flexible [13]. The apo calmodulin NMR structure also reveals that the helical domains adopt a "closed conformation" by packing the hydrophobic residues. This packing is disrupted upon binding Ca^{2+}, altering the structure of each domain and exposing the hydrophobic surfaces for binding to target proteins [14].

The nature of the binding of CaM to Ca^{2+} and to peptides and protein targets was studied by mass spectrometry [15–20], calorimetry [21–23], and fluorescence [24–26]. Those studies reveal that CaM binds Ca^{2+} in a sequential manner when a target protein or peptide is not present [27,28]. Although the two EF hand pairs have ~50% sequence identity and are over 75% sequence similar, the C-terminal domain binds Ca^{2+} with 10-fold higher affinity than the N-terminal domain [4]. CaM undergoes a significant conformational change upon binding Ca^{2+}, consistent with four EF hands that represent nearly 80% of the sequence (29 residues per EF hand and a total of four EF hands). In the presence of protein or pep-

* Corresponding author. Tel.: +1 314 935 4814; fax: +1 314 935 7484.
E-mail address: mgross@wustl.edu (M.L. Gross).
[1] Present address.

1387-3806/$ – see front matter © 2010 Elsevier B.V. All rights reserved.
doi:10.1016/j.ijms.2010.08.013

tide targets, the affinity of CaM for Ca^{2+} (K_i) increases significantly, possibly associated with a slower off-rate (k_{off}) of Ca^{2+} when CaM binds a peptide or another protein [26–28].

We report here H/DX kinetics and PLIMSTEX at the peptide level to determine the site-specific affinity and conformational changes that take place in CaM upon Ca^{2+} binding and subsequent binding to three peptides. Given that the peptides, melittin [29–37], mastoparan [38–46] and MLCK [47–49] interact in a reasonably established way, our principal goal is to establish the outcome of H/DX and PLIMSTEX for studies of metal-containing proteins and their binding to peptides. This extended methodology builds on the global protein analysis reported earlier [20] and offers a higher resolution approach (peptide level) of H/DX kinetics and titrations. To carry out this research, we modified the original PLIMSTEX fitting algorithm [50] to incorporate the high-resolution titration data.

2. Experimental

2.1. Materials

"Calcium-free" porcine calmodulin was from Ocean Biologics Co. (Edmonds, WA). Deuterium oxide, potassium chloride, formic acid, calcium chloride, melittin from honey bee venom (sequence: GIGAVLKVLTTGLPALISWIKRKRQQ, monoisotopic mass 2845.7), mastoparan from *Vespula lewisii* (sequence: INLKALAALAKKIL$_{NH_2}$, monoisotopic mass 1478.0), acetonitrile, EGTA (ethylene glycol-bis(2-aminoethylether)-*N*,*N*,*N*′,*N*′-tetra-acetic acid), HEPES [*N*-(2-hydoxyethyl)piperazine-*N*′-(2-ethanesulfonic acid)], and HEPES sodium salt were from Sigma–Aldrich (St. Louis, MO) and were obtained at the highest purity available. MLCK (sequence: KRRWKKNFIAVSAANRFKKISSSGAL, monoisotopic mass 2962.7) was purchased from AnaSpec (Fremont, CA). Immobilized pepsin on agarose was from Pierce (Rockford, IL). The MW of porcine calmodulin was determined by ESI mass spectrometry to be 16,790 Da (see Supplementary Fig. S-1); this result confirms two post-translational modifications in the calmodulin species, namely N-terminal acetylation (+42 Da) and trimethylation of Lys 115 (+42 Da); these modifications are well-known and common for calmodulin.

2.2. H/D exchange kinetics and titration

Protein stock solutions (238 μM, 1 mg protein in 250 μL buffer) were prepared with 10 mM HEPES (pH 7.4) and 150 mM KCl. A 1:1 dilution of the stock solution was used for each CaM sample of interest, affording an initial CaM concentration of 119 μM in each case. H/DX kinetics experiments were conducted with apo CaM (containing 1 mM EGTA) and holo CaM (containing 2 mM Ca^{2+}). Prior to titration, solutions were equilibrated for 1 h. To initiate exchange, 0.5 μL of the protein stock was diluted with 20 μL of D_2O containing 10 mM HEPES and 150 mM KCl (pD 7.4) at 25 °C to give a solution that was >97% D_2O. After certain times, the exchange was quenched with ice-cold 1.0 M HCl to give a final pH of 2.0.

To examine D uptake for regions of the protein, 5 μL of immobilized pepsin on agarose was added to the quenched solution, digesting the protein for 3 min at 0 °C with a brief vortexing every 15 s. The resulting mixture was briefly centrifuged (2–3 s) so that the beads accumulate at the bottom. The supernatant protein digest, including some undigested protein, was loaded on a C_{18} column (LC Packings, 1 mm × 15 mm, PepMap cartridge, Dionex Corp., Sunnyvale, CA) that was pre-equilibrated with 100 μL of 0.2% formic acid in water (0 °C). The column was washed with 300 μL of 0.2% formic acid in water (0 °C), back exchanging the labile sites of the peptides and protein, and the peptides were separated with a LC gradient (5% B to 40% B in 6 min, 40% B to 75% B in 2 min, 75% B to 5% B in 0.5 min, 5% B to 40% B in 0.5 min, then back to 5% B for equilibration) at a flow rate of 40 μL/min (solvent A: 95% water, 5% acetonitrile containing 0.3% formic acid; solvent B: 5% water, 95% acetonitrile containing 0.3% formic acid). To minimize back exchange, the incoming/outgoing LC solvent line, injection valve, and sample loop were submerged in ice/water slush (0 °C). The deuterium uptake data for one of the component peptides of calmodulin (residues 124–138) are shown in Fig. S-2.

2.3. LC-ESI/MS analysis with a Q-TOF mass spectrometer

All ESI mass spectra during the H/DX experiments were acquired in the positive-ion mode on a Waters (Micromass) Q-TOF Ultima (Manchester, UK) equipped with a Z-spray ESI source. The capillary voltage was 3.2 kV, cone voltage readback of 100 V, and the source and desolvation temperatures were 80 and 180 °C. The cone and desolvation gas flows were 40 and 400 L/h. The MS profile used for quadrupole transmission was from m/z 500, dwell for 5% of the scan time, ramp to m/z 1000 for 45% of the scan time, and then dwell at m/z 1000 for 50% of the scan time.

2.4. LC-ESI/MS–MS analysis of protein digest

After 3 min of pepsin digestion, the solution containing the protein digest, including some undigested protein, was loaded onto a C_{18} custom-packed column (75 μm i.d., 10 cm length). The peptides were separated over 70 min using an Eksigent NanoLC-1D (Dublin, CA) with an LC gradient from 3 to 97% acetonitrile containing 0.1% formic acid at a flow rate of 260 nL/min with spray directly into the mass spectrometer using a PicoView PV-500 nanospray source (New Objective, Woburn, MA) attached to an LTQ-FTMS (Thermo, San Jose, CA), which afforded accurate mass and product-ion sequencing by MS/MS. The peptides were identified by searching against NCBI database on Mascot (Matrix Science, Oxford, UK), and each peptide was manually verified by *de novo* sequencing.

2.5. Data analysis

For H/DX data collected on the Q-TOF, the protein mass spectrum at each exchange time point was deconvoluted with MaxEnt1 algorithm (MassLynx 4.0). The D level at each time point was determined by subtracting the centroided mass of the undeuterated protein from the that of the deuterated protein. The rate of back exchange was 1 D loss per min. Ion signals for the deuterated peptides were smoothed twice in MassLynx with a Savitsky–Golay algorithm and imported into Microsoft Excel as an *x*,*y* pair (mass, intensity). The centroid and width of the deuterium distribution for each peptide was analyzed using HX-Express software [51]. The back exchange occurs at the same rate as in the experiment in which exchange at the global level was examined. No corrections were made for back exchange because only relative D levels were compared. The experiments were in triplicate.

2.6. Kinetic and titration modeling

The H/DX kinetic data were fit with a fixed rate-constant binning model in which all exchangeable H's were separated into four fixed rate-constant bins. The bins were chosen to span four orders of magnitude (10, 1, 0.1, and 0.01 min^{-1}), roughly corresponding to the rate constants that cover the experimental time scale and allowing comparison of the number of exchangeable H's among different binding states of CaM [20]. Specifically, the collected data span from 0.25 to 60 min; hence the brackets of 10 min^{-1} (fast exchangers, half-life ~0.07 min (4 s)) and 0.01 min^{-1} (slow exchangers, half-life

~69 min). We acknowledge that the largest rate constant for H/D exchange is >100 min^{-1} for unstructured peptides [52], but we are yet unable to obtain data at the short times that correspond to this rate constant. Nevertheless, we fit the data with 5 bins, adding a bin at 100 min^{-1}. The outcome is that the number of amides exchanging in the 100 and 10 min^{-1} is the same, within experimental error, as that obtained in the 10 min^{-1} bin when using a four-bin model. There is no significant difference for the number of exchangers in the other rate bins. We are also able to model the kinetic data using various numbers of rate constants as fit parameters, but we chose not to do this because this approach does not facilitate comparisons between various states (e.g., apo vs. holo).

The kinetic model was applied globally to full-length proteins and to component peptides in the digest. The purpose of the model was to monitor qualitatively changes within each bin from sample to sample. The number of exchangeable hydrogens was optimized by using the "Minimize" function in MathCAD to minimize the root mean square (RMS) of the residuals. Each trial (of a total of three) was fit separately, and the results were averaged and reported with ± one standard deviation.

The details of the global titration modeling were described previously [50]. The protocol was modified to utilize the information from titration data at the peptide level. Traditionally, a set of parameters was chosen to fit the experimentally observed data. These included the deuterium uptake with no ligand present (D_0), the deuterium uptake change upon each binding event (ΔD_i), and the affinity constants expressed as β_i's where $\beta_1 = K_{a1}$, $\beta_2 = K_{a1}K_{a2}$, $\beta_3 = K_{a1}K_{a2}K_{a3}$, . . . for each ligand binding event (where i = binding stoichiometry).

The details of the first two Ca^{2+} binding events cannot be resolved on the basis of our titration data, as was described previously [20]. Therefore, the values of K_{a1}, K_{a2}, ΔD_1, and ΔD_2 were held constant during the parameter search. In the modified protocol, the deuterium uptake as $f([Ca^{2+}])$ was input for the full-length protein and the individual constituent peptides. The initial guesses for D_0 and ΔD_4 were set to the experimental values. The non-linear least squares fitting utilized the "Minimize" function in MathCAD to minimize the root mean square (RMS) of all inputs by optimizing the parameters of K_{a3}, K_{a4}, D_0, ΔD_3, and ΔD_4.

3. Results and discussion

3.1. Global H/D exchange kinetics of calmodulin

We found with the pepsin digestion 30–50% protein remained in the digest, probably a result of the low temperature (~0 °C). We took advantage of the incomplete digestion to obtain in the same experiment the D uptake data for the whole protein and for its component peptides. The forward H/DX experiments were conducted over 60 min for (1) CaM with 1 mM EGTA, (2) CaM with 2 mM Ca^{2+}, (3) CaM with 2 mM Ca^{2+} and 2.9:1 ratio of melittin:CaM, and (4) CaM with 2 mM Ca^{2+} and 2.9:1 ratio of mastoparan:CaM, and (5) CaM with 2 mM Ca^{2+} and 2.9:1 ratio of MLCK:CaM. The addition of EGTA ensures that the apo state was essentially 100%, whereas the latter samples contained sufficient Ca^{2+} to ensure that the protein is ~100% Ca^{2+}-bound. Melittin, mastoparan and MLCK all bind calcium-loaded calmodulin at nanomolar affinities [29,38,30,53], ensuring that the peptide/protein complex is fully formed.

A plot of D uptake vs. time shows the protection change of apo CaM upon binding Ca^{2+} in the presence of melittin, mastoparan, and MLCK (Fig. 1). The total number of exchangeable H's for porcine CaM is 146, considering there are two Pro that do not undergo exchange. Given 97% D_2O in all H/DX experiments, the maximum number of observable exchange events is 142. After 10 min of H/DX, apo CaM showed a mass shift of 125.3 ± 0.6 Da, indicating that ~90% of the amide sites were deuterated. This high level of exchange is consistent with the highly flexible and dynamic nature of CaM in the absence of Ca^{2+}. In the presence of Ca^{2+}, the extent of H/DX decreases by 10–15 amides, owing an increase in H bonding throughout CaM (Fig. 1). Upon addition of melittin at a 2.9:1 ratio of CaM in the presence of Ca^{2+}, the extent of H/DX decreases from 109 ± 1 Da to 85 ± 1 Da. A decreased D uptake also occurs upon addition of mastoparan. The corresponding mass shift, from 109 ± 1 Da to 80 ± 1 Da shows that 29 amide sites are affected by mastoparan binding. Although melittin is larger than mastoparan (26 vs. 14 amino acids), the effect of mastoparan binding on HDX of CaM is more pronounced. MLCK (26 amino acids), a similar sized peptide as melittin, also introduces a significant decrease of the extent of H/DX from 109 ± 1 Da to 82 ± 1 Da. This difference is close to that for mastoparan binding, perhaps indicating that the protein complexes share similar structures.

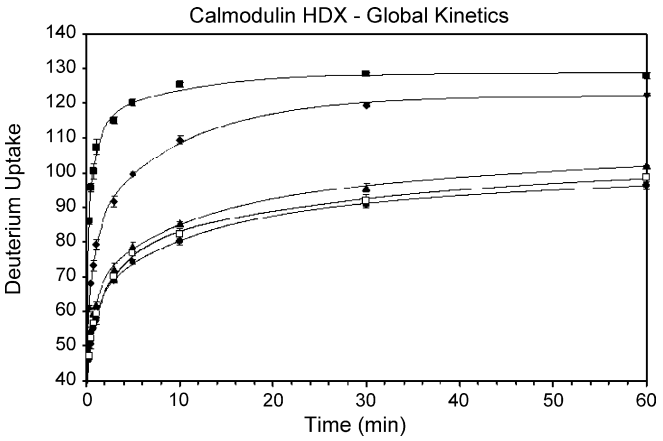

Fig. 1. Global H/DX kinetics experiments: calmodulin with no Ca^{2+} (1 mM EGTA) (squares), calmodulin with 2 mM Ca^{2+} (diamonds), 2.9:1 melittin:calmodulin with 2 mM Ca^{2+} (triangles), 2.9:1 mastoparan:calmodulin with 2 mM Ca^{2+} (circles) and 2.9:1 MLCK:calmodulin with 2 mM Ca^{2+} (open squares). H/DX was conducted over a 60 min time course with 97% D_2O, 10 mM HEPES (pH 7.4), 150 mM KCl, and 2.9 μM calmodulin.

Kinetic modeling (see Table 1; the choices of rate constants and number of bins are rationalized in Section 2.6) reveals that the apo state has 85 sites exchanging with a k = 10 min^{-1} whereas when loaded with Ca^{2+}, the number decreases to 58, indicating that many fast-exchanging amide sites are affected by Ca^{2+} binding. Concomitantly, there is an increase from 15 to 38 that exchange with a rate constant of 0.1 min^{-1}. There are further decreases in the number of exchanging amide hydrogens with a k = 10 min^{-1} upon binding melittin, mastoparan and MLCK. Overall, we see a net shift to lower exchange rate constants for some amides by as much 10^4, consistent with formation of a less flexible, more stabilized secondary structure upon Ca^{2+} and peptide binding.

3.2. H/DX kinetics for regions of calmodulin

Pepsin digestion, which permits exploration of regions of the exchanging protein, affords ~76 unique peptic peptides, which we identified from their product-ion spectra and accurate masses

Table 1
Results of the fixed-rate kinetic binning model for the four kinetics curves in Fig. 1.

Kinetic fit rate (min^{-1})	# H's per fixed-rate bin			
	10	1	0.1	0.01
apo	85 ± 1	28 ± 1	15 ± 1	0 ± 0
holo	58 ± 1	27 ± 1	38 ± 2	0 ± 0
holo w/MEL	48 ± 1	19 ± 3	26 ± 1	20 ± 3
holo w/MAS	43 ± 1	19 ± 2	26 ± 3	18 ± 3
holo w/MLCK	41 ± 1	17 ± 5	25 ± 3	18 ± 1

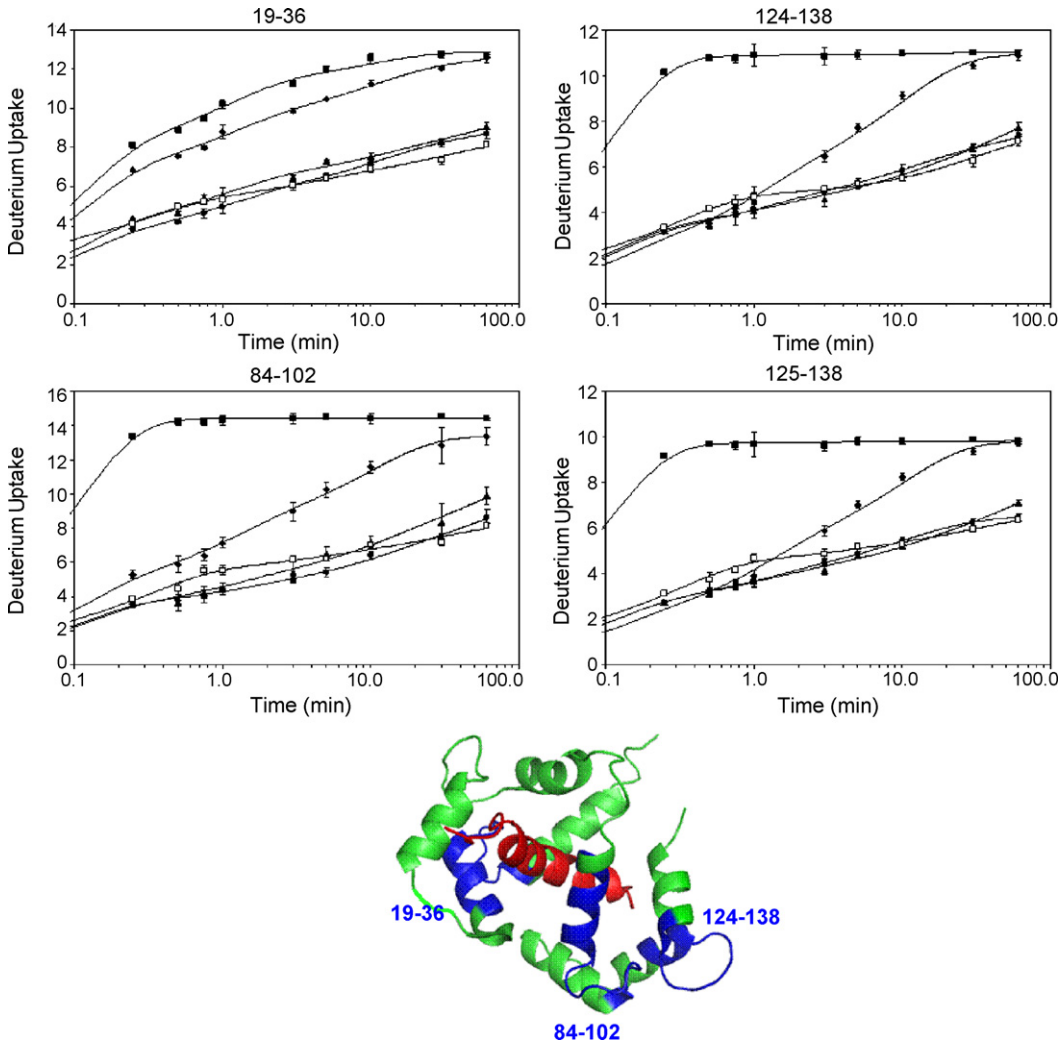

Fig. 2. Local H/DX kinetics in the EF hand regions of CaM. Peptide 19–36 represents EF hand 1, 84–102 represents EF hand 3, and 124–138 and 125–138 represent EF hand 4. Four states are shown: CaM with no Ca^{2+} (squares), CaM with 2 mM Ca^{2+} (diamonds), 2.9:1 melittin:CaM with 2 mM Ca^{2+} (triangles), 2.9:1 mastoparan:CaM with 2 mM Ca^{2+} (circles) and 2.9:1 MLCK:CaM with 2 mM Ca^{2+} (open squares). H/DX was conducted over 60 min with 97% D_2O, 10 mM HEPES (pH 7.4), 150 mM KCl, and 2.9 μM calmodulin. The curves were fit with a four fixed-rate binning model using exchange rate constants of 10, 1 0.1, and 0.01 min^{-1}. The structure of CaM (green):4Ca^{2+} binding to MLCK (red) (PDB: 2BBM) is shown in center. Peptide regions reported here are shown in blue. (For interpretation of the references to color in this figure legend, the reader is referred to the web version of the article.)

(LC/MS/MS with an ion trap/FT mass spectrometer and Mascot analysis). Although we were unable to observe all these peptic peptides with the Q-TOF, most likely because it is less sensitive and was not equipped with nanospray, we found a sufficient number to afford good coverage (~74%). Those peptides identified on the Q-TOF were confirmed by accurate mass and CID fragmentation.

3.3. Extents of HDX for the EF hands

When CaM binds Ca^{2+} at saturating concentrations, the largest changes in H/DX occur for EF hand 3 (residues 84–102) and 4 (residues 124–138, 125–138, and 125–140) (see Fig. 2 kinetic data and structure of the protein/MLCK complex). By way of contrast, EF hand 1 in the N-terminal domain shows only a small change in D uptake upon binding Ca^{2+}. The S/N ratio representing the peptide containing EF hand 2 was insufficient to analyze its D uptake. The region-specific exchange results show that a tighter, less exchangeable structure forms with Ca^{2+} binding in the C-terminal domain. This is consistent with the higher affinity for Ca^{2+} at the C-terminal than at the N-terminal domain [4].

There are also significant changes in D uptake upon binding Ca^{2+} in the presence of melittin, mastoparan and MLCK with respect to Ca^{2+} binding to CaM itself. At 60 min, the largest changes take place in EF hands 1 (peptide 19–36), 3 (peptide 84–102), and 4 (peptides 124–138, 125–138, and 125–140, data not shown for last peptide because it adds no additional insight). Interestingly, melittin, mastoparan and MLCK affect EF hands 1, 3, and 4 similarly, indicating that the Ca^{2+} binding regions do not distinguish these three peptide ligands (i.e., each region becomes comparably stabilized upon binding). Moreover, knowing the structure of 4Ca^{2+}:CaM:MLCK [47], we suggest that the structures of Ca^{2+}-loaded CaM when bound to melittin, mastoparan and MLCK are nearly identical.

3.4. Extents of H/DX in the linker regions

The linker regions between EF hands 1 and 2 (residues 37–48) and between EF hands 3 and 4 (residues 103–112, 103–119, 103–120, and 103–123) (see Fig. 3 for the kinetic data and the structure of the protein/MLCK structure) show relatively little change upon Ca^{2+} binding. There are, however, differences in the D uptakes of peptide 37–48 between the Ca^{2+}-loaded protein with and without a peptide ligand present; binding to a peptide ligand adds additional protection. Similar trends pertain for the linker between EF

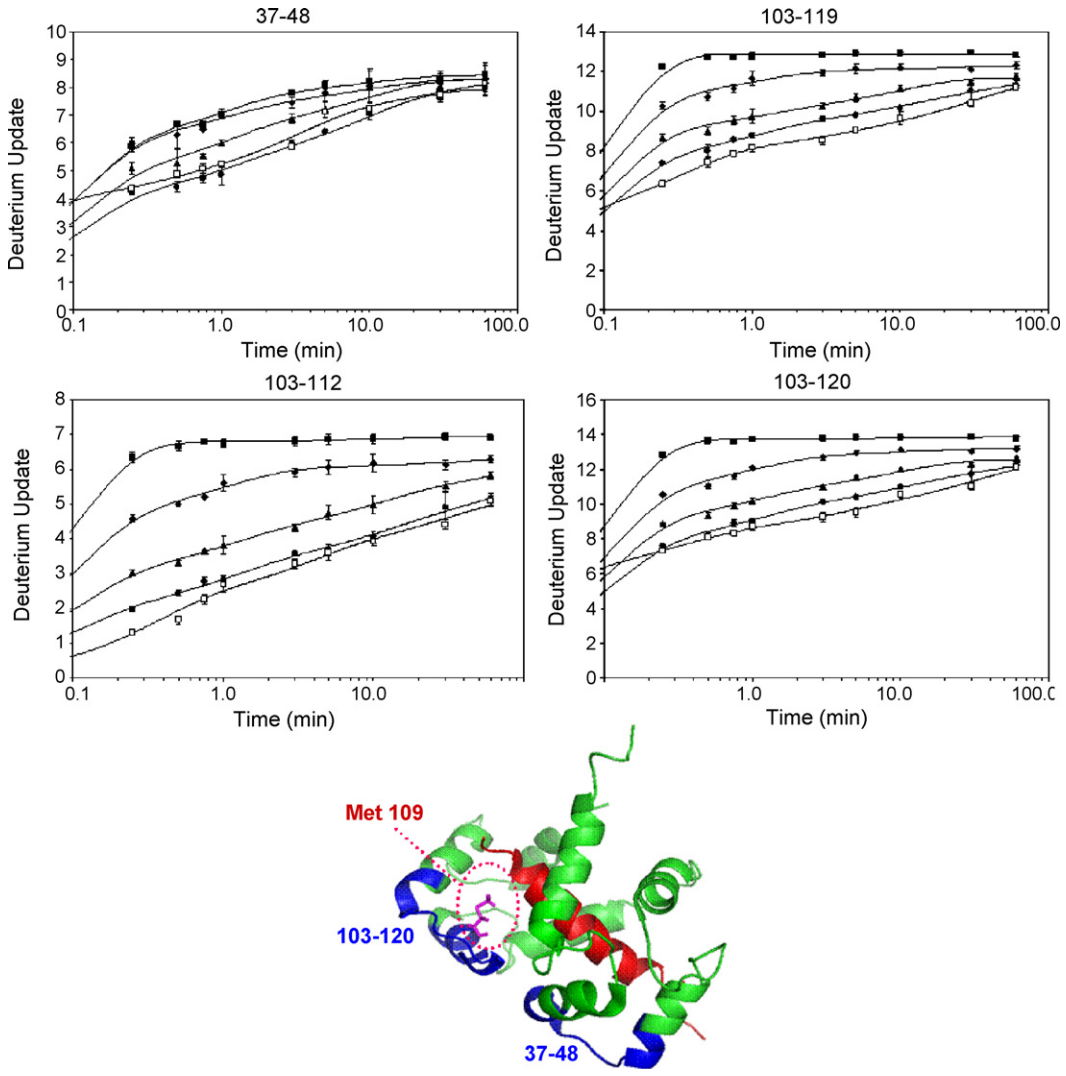

Fig. 3. Local H/D exchange kinetics experiments in the linker regions between EF hands of calmodulin. Peptide 37–48 represents the linker between EF hand 1 and 2 and peptides 103–112, 103–119, 103–120, and 103–123 (not shown) represent the linker between EF hand 3 and 4. Four states of CaM are shown: CaM with no Ca^{2+} (squares), CaM with 2 mM Ca^{2+} (diamonds), 2.9:1 melittin:CaM with 2 mM Ca^{2+} (triangles), 2.9:1 mastoparan:CaM with 2 mM Ca^{2+} (circles) and 2.9:1 MLCK:CaM with 2 mM Ca^{2+} (open squares). Met109 on the CaM structure, shown in pink, is in position to bind peptides. (For interpretation of the references to color in this figure legend, the reader is referred to the web version of the article.)

hands 3 and 4 (peptides 103–112, 103–119, 103–120, and 103–123) when melittin, mastoparan, or MLCK binds to Ca^{2+}-loaded CaM. Mastoparan binding consistently adds protection to one additional amide site upon binding CaM. These linker regions show some specificity for mastoparan over melittin binding, and the approach may ultimately give site-specific peptide-ligand binding.

There are no X-ray or NMR structures of the CaM:4Ca^{2+}:MEL or MAS complexes, but there is an X-ray structure of CaM with the RS20 peptide (RGB ID 1QTX) and, more importantly, an NMR structure of CaM with MLCK (PDB:2BBM) [47] (Figs. 2 and 3). Residues 37–48 and 103–120 of CaM nearly contact one another in the CaM:4Ca^{2+}:MLCK structure even though they are on different domains of calmodulin. The methionines of these two regions of CaM may be involved in binding the peptide ligand. In comparing the extents of D uptake in regions 103–112, 103–119, 103–120, and 103–123, a 1 Da or more difference in deuterium uptake upon binding melittin, mastoparan, and MLCK appears in all the peptic segments. Thus, the incremental protection occurring with the peptide-ligand binding must already occur in region 103–112, which contains Met 109 that is pointing directly at the MLCK peptide in the calmodulin:4Ca^{2+}:MLCK complex structure (Fig. 3).

3.5. Regions of CaM not affected by binding

There are regions of CaM that are little affected by Ca^{2+} binding. Peptides 12–18, 69–72, and, to a lesser extent, peptides 117–128 and 141–148 show only small increases in protection upon binding Ca^{2+}(see supplementary Fig. S-3). Peptide 12–18 is part of the N-terminal tail and EF hand 1, and region 69–72 is the beginning of the central α-helix connecting the two domains. Peptide 117–128 is part of EF hand 4, and 141–148 is the C-terminal tail.

A comparison of the overlap between a region that shows little change upon binding, peptide 117–128, and that showing a significant change, peptide 124–138, reveals that residues 129–138 are those affected by Ca^{2+} binding. These residues are part of EF hand 4.

3.6. Calmodulin binding to Ca^{2+} in the presence or absence of melittin and mastoparan

If there are differences in H/DX between a bound and unbound state of a protein, several H/DX-based methods, including PLIMSTEX, will give the protein's affinity for the ligand [50,54–56]. We

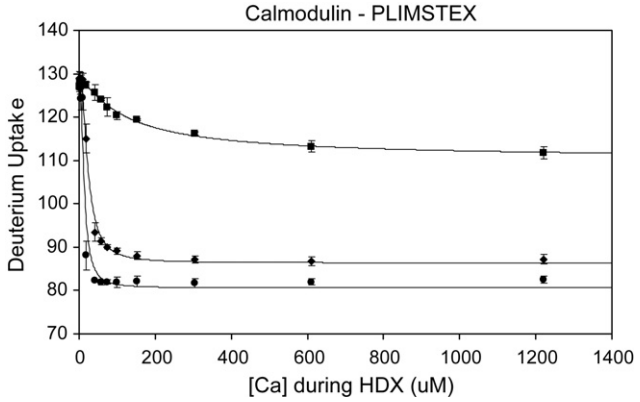

Fig. 4. Global H/DX titration experiments: CaM titrated with Ca^{2+} (squares), 2.9:1 melittin:CaM titrated with Ca^{2+} (diamonds), and 2.9:1 mastoparan:CaM titrated with Ca^{2+} (circles). H/DX was conducted at a constant 10 min with 97% D_2O, 10 mM HEPES (pH 7.4), 150 mM KCl, and 2.9 μM CaM.

chose PLIMSTEX and fit the experimental PLIMSTEX curves (Fig. 4) by a non-linear least squares model to afford the affinity constants of CaM for Ca^{2+}. The best fit determines the D uptake with no Ca^{2+} present (D_0), the deuterium uptake change upon each binding event (ΔD_i), and the affinity constants as β_i's where $\beta_1 = K_{a1}$, $\beta_2 = K_{a1}K_{a2}$, $\beta_3 = K_{a1}K_{a2}K_{a3}$, and $\beta_4 = K_{a1}K_{a2}K_{a3}K_{a4}$. Modeling the titration curve of CaM with Ca^{2+} using a five-parameter search [20] gave D_0, ΔD_3, ΔD_4, β_3, and β_4 (see Table 2). The values of K_{a1} and K_{a2} were fixed at $5.0 \times 10^4\ M^{-1}$ and $1.6 \times 10^6\ M^{-1}$, respectively, for apo CaM titrated with Ca^{2+} [25], and the values of ΔD_1 and ΔD_2 were fixed at 0.

Data from three trials were fit separately to determine the average and standard deviation. The experimental value of D_0 is 127 ± 1 Da, which is in agreement with that from the modeling (i.e., 127 ± 1 Da). The ΔD_{TOT} for CaM titrated with Ca^{2+} is 15 ± 1 Da, in agreement with the modeling (i.e., 17 ± 2 Da). The Ca^{2+} binding affinity from PLIMSTEX, expressed as β_4, is $5 \pm 4 \times 10^{19}\ M^{-4}$ (2.9 μM CaM, 10 mM HEPES, 150 mM KCl, pH 7.4, 25 °C). We determined again this value to test the long-term reproducibility of PLIMSTEX; the β_4 from our previous study is $3.6 \times 10^{19}\ M^{-4}$ (15 μM CaM, 50 mM HEPES, 100 mM KCl, pH 7.4, 21.5 °C) [20]. The value from NMR is $1.6 \times 10^{20}\ M^{-4}$ (20–30 μM CaM, 2 mM Tris/HCl, pH 7.5, 25 °C, 150 mM KCl, and 25–30 μM Br_2BAPTA) [25]. All the results are in good agreement.

The Ca^{2+} binding affinity of CaM and its extent of protection increase dramatically when melittin or mastoparan are present in solution [57–59]. To obtain a fit, the same five-parameter search was used to model the data of CaM binding Ca^{2+} as was used in the absence of melittin and mastoparan with one exception: K_{a1} and K_{a2} were changed to $5.0 \times 10^6\ M^{-1}$ and $1.4 \times 10^6\ M^{-1}$, respectively to reflect the values reported in the literature [32]. These values were determined by tryptophan fluorescence at a lower binding temperature than our protocol (60 μM CaM, 1:1 ratio of CaM:MEL, 20 mM TES buffer, 100 mM NaCl, 1.0 mM EGTA at pH 7.0 and 7 °C). The experimental value of ΔD_{TOT} is 42 ± 1 Da, which agrees with the fit parameter of 44 ± 1 Da, and the new affinity, expressed as β_4, of CaM for Ca^{2+} in the presence of melittin has increased to $1.4 \pm 0.1 \times 10^{22}\ M^{-4}$ (2.9 μM CaM, 10 mM HEPES, and 150 mM KCl). This value agrees reasonably well with that determined previously by us under slightly different conditions; that is, β_4 is $8.0 \times 10^{22}\ M^{-4}$ (15 μM CaM, 50 mM HEPES, and 100 mM KCl) [60]. The binding affinity of CaM for Ca^{2+} in the presence of melittin is 300 times greater than in its absence.

Mastoparan also significantly affects β_4, but this was not reported previously. Our result is $4.3 \pm 0.4 \times 10^{22}\ M^{-4}$ (2.9 μM CaM, 10 mM HEPES, and 150 mM KCl), showing also a significant increase in binding in the presence of mastoparan; β_4 in the presence of mastoparan is nearly 1000 times greater than that without it and three times greater than the affinity in the presence of melittin.

MLCK also increases the β_4; the value is $4.2 \times 10^{22}\ M^{-4}$, as determined by using flow dialysis (5–10 μM CaM, 10 mM HEPES, 150 mM NaCl, and 1 mM $MgCl_2$ at 25 °C) [61]. This value is nearly identical to the β_4 in the presence of mastoparan, as described above. Although we did not measure β_4 for Ca^{2+}-loaded CaM in the presence of MLCK, the H/D kinetics at the global and peptide levels results also show that MLCK affects the binding of CaM with Ca^{2+} in approximately the same way as does mastoparan.

Once the affinity of Ca^{2+} is determined, we calculated the fractionally bound CaM species as a function of Ca^{2+}, giving the concentration of CaM:$x$$Ca^{2+}$ (x = 1–4) species under various conditions. The fourth Ca^{2+} binding event triggers the largest change in D uptake and mimics the overall shape of the observed PLIMSTEX titration curve (see supplementary Fig. S-4). The calculated abundance of the holo CaM species, as indicated by the fourth binding of Ca^{2+}, increases with increasing [Ca^{2+}]. This mimics the overall decrease in H/DX during the PLIMSTEX titration experiment. The relative populations of CaM:1Ca^{2+} and CaM:2Ca^{2+} are relatively small. In the presence of melittin or mastoparan, the binding scenario changes significantly. The CaM:1Ca^{2+} and CaM:3Ca^{2+} are the lowest concentration species, whereas the CaM:2Ca^{2+} is intermediate. This suggests that once the second Ca^{2+} is bound, the third Ca^{2+} begins to bind and then yields to the high-affinity binding of the fourth Ca^{2+}, as revealed by the low concentration of Ca^{2+} needed to form the CaM:4Ca^{2+}:peptide-ligand complex. The fourth binding of Ca^{2+} produces the largest change in D uptake and contributes most to the shape of the observed PLIMSTEX curve for each peptide ligand [20,60].

3.7. Region-specific H/DX titration of calmodulin

Our goal is to advance the PLIMSTEX protocol to a more region-specific approach with the hope of obtaining site-specific affinity constants for any protein of interest. CaM affords an opportunity to test this prospect. CaM has four EF hands, three of which we can liberate by digestion for region-specific H/DX. We were able to follow a subset of eight peptic peptides during the Ca^{2+} titration.

Perhaps the Ca^{2+} binding to each EF hand can be fit with a single affinity constant, treating each site with 1:1 binding stoichiometry. An attempt to do this with EF hand 1 proved unsuccessful (Fig. 5 top). Although the fit is reasonable for Ca^{2+} binding apo calmodulin, it is poor for Ca^{2+} binding in the presence of melittin or mastoparan. The calculated curves from the fitting are shifted to higher concentrations of Ca^{2+}. This shift and the poor agreement indicate that the change in D uptake for this EF hand is not independent of Ca^{2+} binding at other sites, a conclusion that is consistent with findings

Table 2
Output of the PLIMSTEX titration modeling from Fig. 4 using a five-parameter search including D_0, ΔD_3, ΔD_4, β_3, and β_4.

	D_0	ΔD_3	ΔD_4	β_3 ($\times 10^{15}\ M^{-3}$)	β_4 ($\times 10^{19}\ M^{-4}$)
CaM w/Ca^{2+}	127 ± 1	−3.4 ± 2.1	17 ± 2	4 ± 3	5 ± 4
MEL:CaM w/Ca^{2+}	130 ± 1	−0.1 ± 0.0	44 ± 1	0.7 ± 0.1	1350 ± 70
MAS:CaM w/Ca^{2+}	129.0 ± 1.6	0.0 ± 0.0	48.4 ± 1.2	0.7 ± 0.0	4300 ± 400

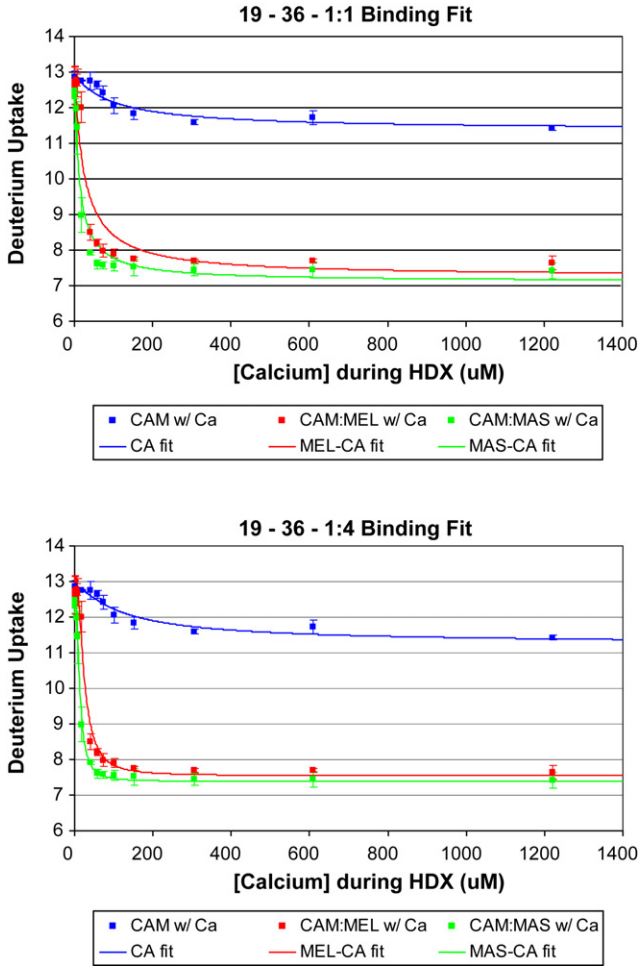

Fig. 5. A comparison of a forced 1:1 fit (top) and the 1:4 fit (bottom) binding model of EF hand 1 (residues 19–36) for the following experiments: calmodulin titrated with Ca^{2+} (squares), 2.9:1 melittin:calmodulin titrated with Ca^{2+} (diamonds), and 2.9:1 mastoparan:calmodulin titrated with Ca^{2+} (circles). The fit for melittin and mastoparan was not successful with a 1:1 binding model. The 1:4 fit, however, models the observed experimental data correctly.

that Ca^{2+} binding to calmodulin is highly cooperative [5]. This same result was obtained for EF hand 4 (data not shown).

The lack of agreement prompted us to modify the existing PLIMSTEX model to incorporate the D uptake of component peptides into the fitting algorithm. Upon fitting the peptide deuterium shift using the four association constants (K_{a1}, K_{a2}, K_{a3}, K_{a4}) from the global data and then minimizing the RMS associated with the ΔD's, we obtained a better fit of EF hand 1 (Fig. 5 bottom), and of peptides representing EF hands 3 and 4 (see supplementary Fig. S-5).

The linker regions (peptides 37–48, 103–112, 103–119, and 103–120) exhibit distinct differences for binding melittin vs. mastoparan (Fig. S-6). A consistent difference of 1 Da is revealed after a minimal addition of Ca^{2+} to the solution. This is consistent with H/DX kinetics at the peptic peptide level.

The modified PLIMSTEX model utilizes the deuterium shifts observed in the protein and peptide-ligand titration curves simultaneously, iterating through each to determine the affinity parameters. The expanded array of data improves the RMS of the global titration curve, most likely due to statistical power, when calmodulin is titrated with Ca^{2+}. The RMS decreases from 0.40 to 0.16 for the apo CaM:Ca^{2+} titration. In this case the affinity output was different, whereas β_4 from protein data is $4.0 \times 10^{18}\,M^{-4}$, the inclusion of the expanded array was $4.5 \times 10^{19}\,M^{-4}$, an order of magnitude different. In the presence of melittin, the affinity (β_4) was the same ($1.4 \times 10^{22}\,M^{-4}$), however the RMS decreased from 1.7 to 0.6. In the presence of mastoparan, the affinity (β_4) was the same ($4.3 \times 10^{22}\,M^{-4}$). The RMS, however, decreased from 4.1 to 1.4, presumably because nine curves (one global and eight peptide level), instead of one global protein curve, were monitored. Furthermore, peptide MWs are more accurately measured than are protein MWs.

4. Conclusion

HD/X at the protein and component peptide levels, utilizing kinetics and PLIMSTEX, affords a detailed binding picture of calmodulin binding to Ca^{2+}. The presence of Ca^{2+} induces a conformational change observed in the EF hand regions that can be characterized by an overall stabilization of their secondary structures. In the presence of three model peptide ligands, melittin, mastoparan, and MLCK, calmodulin changes even more its conformation when a Ca^{2+} signal is introduced. Each peptide ligand affords similar effects in deuterium uptake in the EF hand regions. The linker regions, on the other hand, show some specificity for mastoparan and MLCK, indicated by an increase in protection. These regions are known to contain hydrophobic residues that affect the extensive binding network of CaM. Incorporating the component peptide titration data affords better fits for the affinity constants and changes in D uptake with ligand binding, suggesting a general approach to improve the accuracy and precision of PLIMSTEX. Although CaM has been studied extensively, the results presented here indicate that PLIMSTEX is a useful approach for these metal-binding EF hand regions and that it can add to our knowledge about cooperativity in higher order binding systems. Moreover, the outcome shows that ligand/protein binding in the presence of potential binding partners, as it is in vivo, may be surprisingly different than ligand/protein alone in aqueous solution, the usual medium for biophysical measurements.

Acknowledgement

This research was supported by the National Center of Research Resources of the NIH, Grant no. 2P41RR000954.

Appendix A. Supplementary data

Supplementary data associated with this article can be found, in the online version, at doi:10.1016/j.ijms.2010.08.013.

References

[1] J. Evenäs, A. Malmendal, S. Forsén, Calcium, Current Opinion in Chemical Biology 2 (1998) 293–302.
[2] M. Brini, E. Carafoli, Calcium signalling: a historical account, recent developments and future perspectives, Cellular and Molecular Life Sciences 57 (2000) 354–370.
[3] E Carafoli, Calcium signaling: a tale for all seasons, Proceedings of the National Academy of Sciences 99 (2002) 1115–1122.
[4] S.W. Vetter, E. Leclerc, Novel aspects of calmodulin target recognition and activation, European Journal of Biochemistry 270 (2003) 404–414.
[5] J.J. Yang, A. Gawthrop, Y. Ye, Obtaining site-specific calcium-binding affinities of calmodulin, Protein and Peptide Letters 10 (2003) 331–345.
[6] S. Kakiuchi, R. Yamazaki, Stimulation of the activity of cyclic 3′,5′-nucleotide phosphodiesterase by calcium ion, Proceedings of the Japan Academy 46 (1970) 387–392.
[7] W.Y. Cheung, Cyclic 3′,5′-nucleotide phosphodiesterase. Demonstration of an activator, Biochemical and Biophysical Research Communications 38 (1970) 533–538.
[8] J.H. Wang, D.M. Waisman, Calmodulin and its role in the second-messenger system, Current Topics in Cellular Regulation 15 (1979) 47–107.
[9] D.J. Wolff, C.O. Brostrom, Properties and functions of the calcium-dependent regulator protein, Advances in Cyclic Nucleotide Research 11 (1979) 27–88.
[10] R.H. Kretsinger, C.E. Nockolds, Carp-muscle calcium-binding protein, Journal of Biological Chemistry 248 (1973) 3313–3326.

[11] Y.S. Babu, J.S. Sack, T.J. Greenhough, C.E. Bugg, A.R. Means, W.J. Cook, Three-dimensional structure of calmodulin, Nature 315 (1985) 37–40.
[12] Y.S. Babu, C.E. Bugg, W.J. Cook, Structure of calmodulin refined at 2.2 A resolution, Journal of Molecular Biology 204 (1988) 191–204.
[13] H. Kuboniwa, N. Tjandra, S. Grzesiek, H. Ren, C.B. Klee, A. Bax, Solution structure of calcium-free calmodulin, Nature Structural and Molecular Biology 2 (1995) 768–776.
[14] M. Zhang, T. Yuan, Molecular mechanisms of calmodulin's functional versatility, Biochemistry and Cell Biology 76 (1998) 313–323.
[15] P. Hu, Q.-Z. Ye, J. Loo, Calcium stoichiometry determination for calcium binding proteins by electrospray ionization mass spectrometry, Analytical Chemistry 66 (1994) 4190–4194.
[16] D. Lafitte, J.P. Capony, G. Grassy, J. Haiech, B. Calas, Analysis of the ion binding sites of calmodulin by electrospray ionization mass spectrometry, Biochemistry 34 (1995) 13825–13832.
[17] O. Nemirovskiy, R. Ramanathan, M.L. Gross, Investigation of calcium-induced, noncovalent association of calmodulin with melittin by electrospray ionization mass spectrometry, Journal of the American Society for Mass Spectrometry 8 (1997) 809–812.
[18] M Nousiainen, P. Vainiotalo, X. Feng, P.J. Derrick, Calmodulin–Rs20–Ca4 complex in the gas phase: electrospray ionization and Fourier transform ion cyclotron resonance, European Journal of Mass Spectrometry 7 (2001) 393–398.
[19] R.F. Steiner, S. Albaugh, C. Fenselau, C. Murphy, M. Vestline, A mass spectrometry method for mapping the interface topography of interacting proteins, illustrated by the melittin–calmodulin system, Analytical Biochemistry 196 (1991) 120–125.
[20] M.M Zhu, D.L. Rempel, J. Zhao, D.E. Giblin, M.L. Gross, Probing Ca^{2+}-induced conformational changes in porcine calmodulin by H/D exchange and ESI-MS: effect of cations and ionic strength, Biochemistry 42 (2003) 15388–15397.
[21] R.D. Brokx, M.M. Lopez, H.J. Vogel, G.I. Makhatadze, Energetics of target peptide binding by calmodulin reveals different modes of binding, Journal of Biological Chemistry 276 (2001) 14083–14091.
[22] R. Gilli, D. Lafitte, C. Lopez, M.-C. Kilhoffer, A. Makarov, C. Briand, J. Haiech, Thermodynamic analysis of calcium and magnesium binding to calmodulin, Biochemistry 73 (1998) 5450–5456.
[23] M. Milos, J.J. Schaer, M. Comte, J.A. Cox, Calcium-proton and calcium–magnesium antagonisms in calmodulin: microcalorimetric and potentiometric analyses, Biochemistry 25 (1986) 6279–6287.
[24] W.S. VanScyoc, M. Shea, Phenylalanine fluorescence studies of calcium binding to N-domain fragments of paramecium calmodulin mutants show increased calcium affinity correlates with increased disorder, Protein Science 10 (2001) 1758–1768.
[25] S. Linse, A. Helmersson, S. Forsén, Calcium binding to calmodulin and its globular domains, Journal of Biological Chemistry 266 (1991) 8050–8054.
[26] M.-C. Kilhoffer, J.G. Demaille, D. Gerard, Tyrosine fluorescence of ram testis and octopus calmodulins. Effects of calcium, magnesium, and ionic strength, Biochemistry 20 (1981) 4407–4414.
[27] M.-C. Kilhoffer, M. Kubina, F. Travers, J. Haiech, Use of engineered proteins with internal tryptophan reporter groups and perturbation techniques to probe the mechanism of ligand–protein interactions: investigation of the mechanism of calcium binding to calmodulin, Biochemistry (1992) 8098–8106.
[28] J. Haiech, C.B. Klee, J.G. Demaille, J. Haiech, Effects of cations on affinity of calmodulin for calcium: ordered binding of calcium ions allows the specific activation of calmodulin-stimulated enzymes. Theoretical approach to the study of multiple ligand binding to a macromolecule, Biochemistry (1981) 3890–3897.
[29] M. Comte, Y. Maulet, J.A. Cox, Ca^{2+}-dependent high-affinity complex formation between calmodulin and melittin, Biochemical Journal 209 (1983) 269–272.
[30] Y. Yao, T.C. Squier, Variable conformation and dynamics of calmodulin complexed with peptides derived from the autoinhibitory domains of target proteins, Biochemistry 35 (1996) 6815–6827.
[31] T.C. Terwilliger, L. Weissman, D. Eisenberg, The structure of melittin in the form I crystals and its implication for melittin's lytic and surface activities, Biophysical Journal 37 (1982) 353–361.
[32] Y. Maulet, J.A. Cox, Structural changes in melittin and calmodulin upon complex formation and their modulation by calcium, Biochemistry 22 (1983) 5680–5686.
[33] D.M. Schulz, C. Ihling, G.M. Clore, A. Sinz, Mapping the topology and determination of a low-resolution three-dimensional structure of the calmodulin–melittin complex by chemical cross-linking and high-resolution FTICRMS: direct demonstration of multiple binding modes, Biochemistry 43 (2004) 4703–4715.
[34] A. Scaloni, N. Miraglia, S. Orru, P. Amodeo, A. Motta, G. Marino, P. Pucci, Topology of the calmodulin–melittin complex, Journal of Molecular Biology 277 (1998) 945–958.
[35] C.G. Caday, R.F. Steiner, The interaction of calmodulin with melittin, Biochemical and Biophysical Research Communications 135 (1986) 419–425.
[36] M. Kataoka, J.F. Head, B.A. Seaton, D.M. Engelman, Melittin binding causes a large calcium-dependent conformational change in calmodulin, Proceedings of the National Academy of Sciences 86 (1989) 6944–6948.
[37] S. Mathur, M. Badertscher, M. Scott, R. Zenobi, Critical evaluation of mass spectrometric measurement of dissociation constants: accuracy and cross-validation against surface plasmon resonance and circular dichroism for the calmodulin–melittin system, Physical Chemistry Chemical Physics 9 (2007) 6187–6198.
[38] D.A. Malencik, S.R. Anderson, High affinity binding of the mastoparans by calmodulin, Biochemical and Biophysical Research Communications 114 (1983) 50–56.
[39] D.A. Malencik, S.R. Anderson, Demonstration of a fluorometrically distinguishable intermediate in calcium binding by calmodulin–mastoparan complexes, Biochemical and Biophysical Research Communications 135 (1986) 1050–1057.
[40] M. Yazawa, M. Ikura, K. Hikichi, L. Ying, K. Yagi, Communication between two globular domains of calmodulin in the presence of mastoparan or caldesmon fragment, Journal of Biological Chemistry 262 (1987) 10951–10954.
[41] N. Matsushima, Y. Izumi, T. Matsuo, H. Yoshino, T. Ueki, Y. Miyake, Binding of both Ca^{2+} and mastoparan to calmodulin induces a large change in the tertiary structure, Journal of Biochemistry 105 (1989) 883–887.
[42] H. Yoshino, O. Minari, N. Matsushima, T. Ueki, Y. Miyake, T. Matsuo, Y. Izumi, Calcium-induced shape change of calmodulin with mastoparan studied by solution X-ray scattering, Journal of Biological Chemistry 264 (1989) 19706–19709.
[43] S.-y. Ohki, M. Yazawa, K. Yagi, K. Hikichi, Mastoparan binding induces Ca^{2+}-transfer between two globular domains of calmodulin: a proton NMR study, Journal of Biochemistry 110 (1991) 737–742.
[44] S.-y. Ohki, S. Tsuda, S. Joko, M. Yazawa, K. Yagi, K. Hikichi, ^{1}H NMR study on amide proton exchange of calmodulin–mastoparan complex, Journal of Biochemistry 109 (1991) 234–237.
[45] T. Wolf, B. Solomon, D. Ivnitski, J. Rishpon, G. Fleminger, Interactions of calmodulin with metal ions and with its target proteins revealed by conformation-sensitive monoclonal antibodies, Journal of Molecular Recognition 11 (1998) 14–19.
[46] A.K. Moorthy, B. Gopal, P.R. Satish, S. Bhattacharya, A. Bhattacharya, M.R.N. Murthy, A. Surolia, Thermodynamics of target peptide recognition by calmodulin and a calmodulin analogue: implications for the role of the central linker, FEBS Letters 461 (1999) 19–24.
[47] G.M.C. Mitsuhiko Ikura, A.M. Gronenborn, G. Zhu, C.B. Klee, A. Bax, Solution structure of a calmodulin-target peptide complex by multidimensional NMR, Science 256 (1992) 632–638.
[48] C. Hultschig, H.-J.g. Hecht, R. Frank, Systematic delineation of a calmodulin peptide interaction, Journal of Molecular Biology 343 (2004) 559–568.
[49] A.F. Wendy, J.G. Michael, M.B. Peter, Role of the N-terminal region of the skeletal muscle myosin light chain kinase target sequence in its interaction with calmodulin, Protein Science 4 (1995) 2375–2382.
[50] M.M. Zhu, D.L. Rempel, M.L. Gross, Modeling data from titration, amide H/D exchange, and mass spectrometry to obtain protein–ligand binding constants, Journal of the American Society for Mass Spectrometry 15 (2004) 388–397.
[51] D.D Weis, J.R. Engen, I.J. Kass, Semi-automated data processing of hydrogen exchange mass spectra using *HX-Express*, Journal of the American Society for Mass Spectrometry 17 (2006) 1700–1703.
[52] Y. Bai, J.S. Milne, L. Mayne, S.W. Englander, Primary structure effects on peptide group hydrogen exchange, Proteins: Structure, Function, and Bioinformatics 17 (1993) 75–86.
[53] C.-F. Zheng, T. Simcox, L. Xu, P. Vaillancourt, A new expression vector for high level protein production, one step purification and direct isotopic labeling of calmodulin-binding peptide fusion proteins, Gene 186 (1997) 55–60.
[54] M.M Zhu, D.L. Rempel, Z. Du, M.L. Gross, Quantification of protein–ligand interactions by mass spectrometry, titration, and H/D exchange: PLIMSTEX, Journal of the American Chemical Society 125 (2003) 5252–5253.
[55] L. Tang, E.D. Hopper, Y. Tong, J.D. Sadowsky, K.J. Peterson, S.H. Gellman, M.C. Fitzgerald, H/D exchange- and mass spectrometry-based strategy for the thermodynamic analysis of protein–ligand binding, Analytical Chemistry 79 (2007) 5869–5877.
[56] H. Xiao, I.A. Kaltashov, S.J. Eyles, Indirect assessment of small hydrophobic ligand binding to a model protein using a combination of ESI MS and HDX/ESI MS, Journal of the American Society for Mass Spectrometry 14 (2003) 506–515.
[57] M. Yazawa, M. Ikura, K. Hikichi, L. Ying, K. Yagi, Communication between two globular domains of calmodulin in the presence of mastoparan or caldesmon fragment. Ca^{2+} binding and ^{1}H NMR, Journal of Biological Chemistry 262 (1987) 10951–10954.
[58] A.N. Rhonda, S.V.S. Wendy, R.S. Brenda, R.J. Olav, A.S. Madeline, Interdomain cooperativity of calmodulin bound to melittin preferentially increases calcium affinity of sites I and II, Proteins: Structure, Function, and Bioinformatics 71 (2008) 1792–1812.
[59] P.M. Bayley, W.A. Findlay, S.R. Martin, Target recognition by calmodulin: dissecting the kinetics and affinity of interaction using short peptide sequences, Protein Science 5 (1996) 1215–1228.
[60] M.M. Zhu, Determination of Protein–ligand Interactions using H/D Exchange and Mass Spectrometry, Chemistry, Washington University, St. Louis, 2004, p. 358.
[61] Y.K. Persechini Anthony, M. Stemmer Paul, Ca^{2+} binding and energy coupling in the calmodulin-myosin light chain kinase complex, Journal of Biological Chemistry 275 (2000) 4199–4204.